

# Single-spin measurement and decoherence in magnetic-resonance force microscopy

G. P. Berman,<sup>1</sup> F. Borgonovi,<sup>1,2</sup> Hsi-Sheng Goan,<sup>3</sup> S. A. Gurvitz,<sup>4</sup> and V. I. Tsifrinovich<sup>5</sup>

<sup>1</sup>*Theoretical Division and CNLS, Los Alamos National Laboratory, Los Alamos, New Mexico 87545*

<sup>2</sup>*Dipartimento di Matematica e Fisica, Università Cattolica, via Musei 41, 25121 Brescia, Italy;*

*INFN, Unità di Brescia, Brescia, Italy;*

*and INFN, Sezione di Pavia, Pavia, Italy*

<sup>3</sup>*Center for Quantum Computer Technology, University of New South Wales, Sydney, NSW 2052, Australia*

<sup>4</sup>*Department of Particle Physics, Weizmann Institute of Science, Rehovot 76100, Israel*

<sup>5</sup>*IDS Department, Polytechnic University, Six Metrotech Center, Brooklyn, New York 11201*

(Received 12 September 2002; published 27 March 2003)

We consider a simple version of a cyclic adiabatic inversion (CAI) technique in magnetic-resonance force microscopy (MRFM). We study the problem: What component of the spin is measured in the CAI MRFM? We show that the nondestructive detection of the cantilever vibrations provides a measurement of the spin component along the effective magnetic field. This result is based on numerical simulations of the Hamiltonian dynamics (the Schrödinger equation) and the numerical solution of the master equation.

DOI: 10.1103/PhysRevB.67.094425

PACS number(s): 76.60.-k, 03.65.Ta, 03.67.Lx

## I. INTRODUCTION

Magnetic-resonance force microscopy (MRFM) is striving for its ultimate goal: single-spin detection.<sup>1-3</sup> The most promising approach to single-spin detection is, probably, cyclic adiabatic inversion (CAI).<sup>1</sup> In this approach, the magnetic moment of the sample changes its direction adiabatically following the effective magnetic field. The CAI of the spin may act as an “external force” driving the resonant vibrations of the cantilever or it may affect the frequency of the cantilever vibrations driven by another source [e.g., the modern “OSCAR” (oscillating cantilever-driven adiabatic reversal) technique<sup>3</sup>].

The fundamental question which arises in MRFM single-spin measurement is the following: What component of the spin is measured by this technique? Indeed, in a simple geometry, the cantilever tip oscillating along the  $z$  axis interacts with the  $z$  component of the spin and, consequently, is expected to measure the spin  $z$  component. From the other side, adiabatic inversion assumes that the approximate integral of motion is the spin component along the effective magnetic field which rotates in the  $x$ - $z$  plane. Thus, one might expect that the cantilever measures the spin component along the effective magnetic field in the rotating reference frame.

In this work, we consider the macroscopic cantilever itself as the measuring device interacting with an environment. We assume that the influence of an additional (e.g., optical) device that detects the cantilever vibrations is small. This corresponds to the current MRFM technique. In Sec. II, we discuss the quantum dynamics of the quasiclassical cantilever which describes the generation of Schrödinger cat states associated with two possible projections of the spin. In Sec. III, we include the interaction of the cantilever with an environment inherent to any measurement processes. The latter leads to the decoherence of the two possible cantilever trajectories.

## II. HAMILTONIAN DYNAMICS

We consider the simple setup shown in Fig. 1.

The ferromagnetic particle with a magnetic moment  $\vec{m}$  is mounted on the cantilever tip. The permanent magnetic field

$B_0$  points in the positive  $z$  direction. A rotating rf field in the  $x$ - $y$  plane,  $\vec{B}_1 \sim \exp(i[\omega t - \varphi(t)])$ , is resonant with the spin precession around the  $z$  axis. The frequency modulation of  $\vec{B}_1$  causes the CAI of the spin. Under resonant conditions, when the period of the cantilever vibrations matches the period of the CAI, the amplitude of the cantilever vibrations is expected to increase providing the detection of the spin.

The quantum Hamiltonian of the system in the rotating frame (in terms of dimensionless parameters) can be written as

$$\mathcal{H} = (p_z^2 + z^2)/2 + \dot{\varphi}(\tau)S_z - \epsilon S_x - 2\eta z S_z. \quad (1)$$

Here

$$p_z = P_z/P_q, \quad z = Z/Z_q, \quad (2)$$

$\vec{S}$  is the electron-spin operator,  $\epsilon = \gamma B_1/\omega_c$ ,  $\dot{\varphi} = d\varphi/d\tau$ ,  $\eta = gF/2F_q$ ,  $P_z$  and  $Z$  are the operators of the electron momentum and coordinate of the cantilever tip,  $\gamma = g\mu_B/\hbar$  is the spin gyromagnetic ratio (absolute value),  $\omega_c$  is the cantilever frequency, and  $F$  is the magnetic force between the ferromagnetic particle and the spin when the cantilever tip is at the origin  $z=0$ . The origin is chosen at the equilibrium position of the cantilever with no spin;  $\tau = \omega_c t$  is a dimensionless time. The units of the coordinate, momentum, and force are given by

$$Z_q = (\hbar\omega_c/k_c)^{1/2}, \quad P_q = \hbar/Z_q, \quad F_q = k_c Z_q, \quad (3)$$

where  $k_c$  is the cantilever spring constant. Note that we treat the electron spin of a paramagnetic atom whose direction is opposite to the direction of the atomic magnetic moment. We assume in Eq. (1) that the transverse magnetic field points in the negative  $x$  direction of the rotating frame.

With respect to actual “reading” devices, we consider a realistic scenario for the MRFM technique which involves nondestructive measurements of the amplitude, frequency, and phase of the cantilever vibrations, for example, by using a fiber-optic interferometer operating in the infrared region. We assume that the optical detection of cantilever vibrations does not influence significantly the cantilever-spin dynamics.

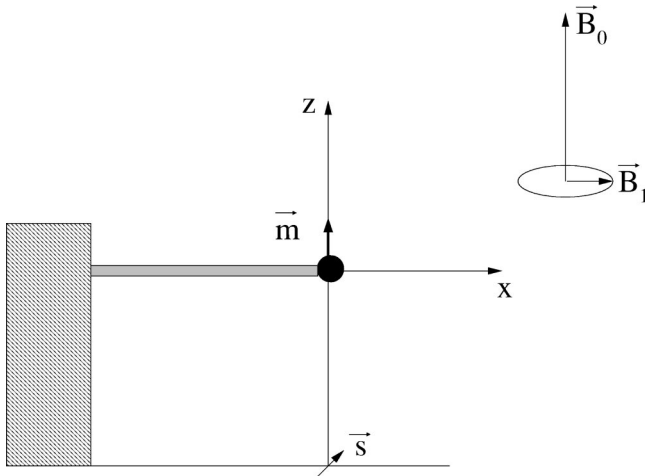


FIG. 1. MRFM setup.

(In practice, this means that the disturbance caused by the optical radiation is smaller than the thermal noise of the cantilever.)

In this section, we do not consider the interaction with the environment which provides the measurement itself. (See also Ref. 4.) Thus, we use the Schrödinger equation

$$i\dot{\Psi} = \mathcal{H}\Psi \quad (4)$$

for computer simulations of the cantilever-spin dynamics. In the  $z$ - $S_z$  representation, the wave function  $\Psi$  is a spinor. It contains two components  $\Psi(z, 1/2, \tau)$  and  $\Psi(z, -1/2, \tau)$ , which correspond to the two possible values of  $S_z$ . Using the expansion over the eigenfunctions  $u_n$  of the oscillator Hamiltonian  $(p_z^2 + z^2)/2$  we write these two components of the cantilever-spin wave function in the form

$$\begin{aligned} \Psi(z, 1/2, \tau) &= \sum_{n=0}^{\infty} A_n(\tau) u_n, \\ \Psi(z, -1/2, \tau) &= \sum_{n=0}^{\infty} B_n(\tau) u_n, \end{aligned} \quad (5)$$

and derive equations for the amplitudes,  $A_n$  and  $B_n$ ,

$$\begin{aligned} i\dot{A}_n &= (n+1/2 + \dot{\varphi}/2)A_n - (\eta/\sqrt{2})(\sqrt{n}A_{n-1} + \sqrt{n+1}A_{n+1}) \\ &\quad - (\epsilon/2)B_n, \\ i\dot{B}_n &= (n-1/2 + \dot{\varphi}/2)B_n + (\eta/\sqrt{2})(\sqrt{n}B_{n-1} + \sqrt{n+1}B_{n+1}) \\ &\quad - (\epsilon/2)A_n. \end{aligned} \quad (6)$$

The initial conditions describe the quasiclassical state of the cantilever tip and a spin which points in the positive  $z$  direction,

$$\begin{aligned} A_n(0) &= (\alpha^n / \sqrt{n!}) \exp(-|\alpha|^2/2), \quad B_n(0) = 0, \\ \alpha &= [\langle z(0) \rangle + i\langle p_z(0) \rangle] / \sqrt{2}. \end{aligned} \quad (7)$$

In our computer simulations we used the following parameter values:

$$\eta = 0.3, \quad \epsilon = 400, \quad \dot{\varphi} = -6000 + 300\tau \quad \text{when } \tau \leq 20 \quad (8)$$

$$\text{and } \dot{\varphi} = 1000 \sin(\tau - 20) \quad \text{when } \tau > 20.$$

The value  $\eta = 0.3$  can be achieved in current MRFM experiments.<sup>1-3</sup> The parameters for the transverse magnetic field have been chosen to satisfy two conditions. (i) the condition of the CAI,  $|\dot{\varphi}| \ll \epsilon^2$  and (ii) the effective magnetic field produced by the cantilever vibrations on the spin is small in comparison with the amplitude of the  $rf$  field:  $2\eta|\langle z \rangle| \ll \epsilon$ . We consider the results of the computer simulations reliable if they do not change with an increase in the number of basic functions  $u_n$ .

To describe the quasiclassical cantilever, we took the initial average energy  $\langle E(0) \rangle = |\alpha|^2 \gg 1$ . The number of basic functions  $u_n$ , needed to provide reliable results, increases with the average energy. So, we cannot take  $|\alpha|$  too large. As we study the driven oscillations of the cantilever, our results do not show a significant dependence on the initial conditions.

The main results of our simulations are the following. The wave function of the cantilever-spin system, which is initially a product of the cantilever and spin parts, quickly becomes entangled. The probability distribution to find the cantilever at the point  $z$  at time  $\tau$ ,

$$P(z, \tau) = |\Psi(z, 1/2, \tau)|^2 + |\Psi(z, -1/2, \tau)|^2 \quad (9)$$

splits into two peaks, “big” and “small” peaks. (See Fig. 2.) When the peaks are separated, the wave function of the cantilever-spin system can be represented as a sum of two spinors,

$$\Psi(z, s, \tau) = \Psi^{(1)}(z, s, \tau) + \Psi^{(2)}(z, s, \tau), \quad (10)$$

where the upper indices “1” and “2” refer to the big and the small peaks, correspondingly. It was found with the accuracy to 1% that both spinor wave functions,  $\Psi^{(k)}(z, s, \tau)$  ( $k = 1, 2$ ), can be represented as a product of the cantilever and spin functions,

$$\Psi^{(k)}(z, s, \tau) = R^{(k)}(z, \tau) \chi^{(k)}(s, \tau), \quad (11)$$

where  $\chi^{(1)}(s, \tau)$  describes the spin that points in the direction of the external effective field,  $[\epsilon, 0, -\dot{\varphi}(\tau)]$ , and  $\chi^{(2)}(s, \tau)$  describes the spin that points in the opposite direction. The ratio of the probabilities for the big and the small peak is determined by the initial angle between the external effective magnetic field and the spin,

$$\int |R^{(2)}(z, \tau)|^2 dz \Big/ \int |R^{(1)}(z, \tau)|^2 dz = \tan^2(\Theta/2), \quad (12)$$

where  $\Theta$  is the initial direction of the external effective magnetic field [ $\tan \Theta = -\epsilon/\dot{\varphi}(0) = 1/15$ ]. If the initial conditions describe a spin that points, for example, in the positive  $x$  direction [ $A_n(0) = B_n(0)$ ], our simulations reveal two peaks with approximately equal amplitudes. Thus, the Hamiltonian dynamics clearly indicates that the quasiclassical cantilever will measure the spin component along the effective magnetic field. Certainly, in the frame of the Hamiltonian ap-

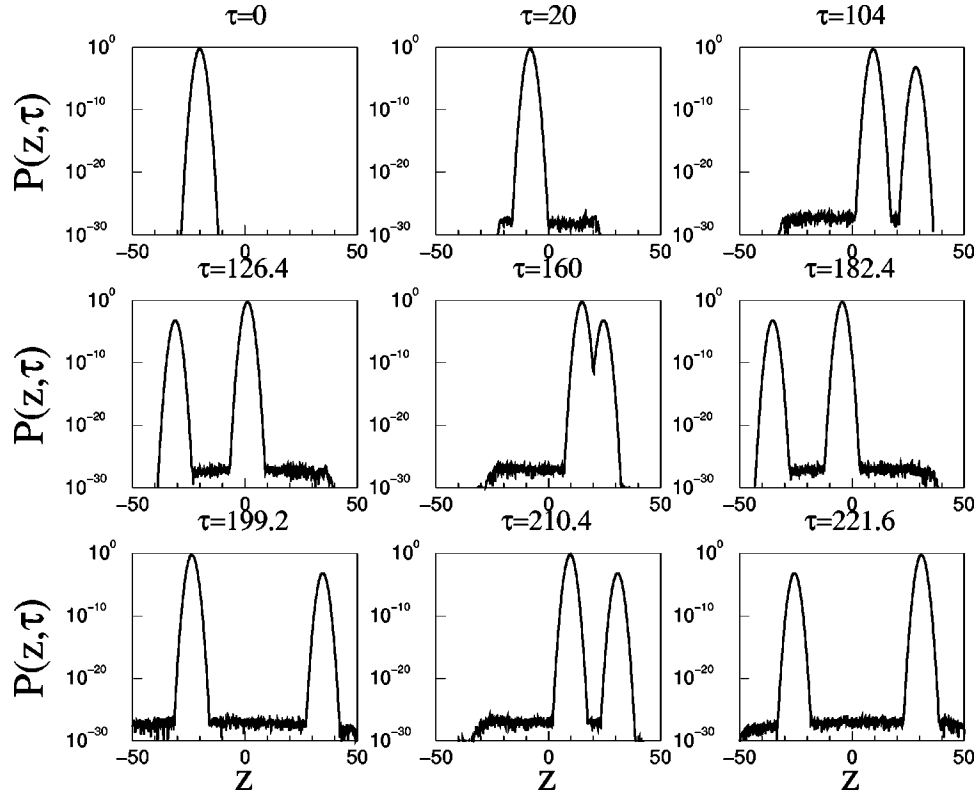


FIG. 2. The probability distribution  $P(z, \tau)$  for the cantilever position in the logarithmic scale for nine different times as indicated in the legend. The values of parameters are  $\epsilon=400$  and  $\eta=0.3$ . The initial conditions are  $\langle z(0) \rangle = -20$ ,  $\langle p_z(0) \rangle = 0$  (which corresponds to  $\alpha = -10\sqrt{2}$ ).

proach, we cannot describe the measurement itself: the coherence between the two cantilever peaks does not disappear. In other words, the Schrödinger equation describes the macroscopic Schrödinger cat state of the cantilever without effects of decoherence.

### III. MASTER EQUATION

In the preceding section, we have presented indications that the cantilever “measures” the spin component along the direction of the effective magnetic field. In this section we describe the measurement process. During the measurement process, the coherence between the two cantilever trajectories disappears. It means that the reduced density matrix of the cantilever-spin system becomes a statistical mixture representing two possible trajectories of the system. The main question we are going to answer is the following: Does the cantilever, which interacts with the environment, measure the spin component along the effective magnetic field?

To answer this question, we studied the dynamics of the cantilever-spin system using the master equation. Our purpose is not just to simulate the expected experiment but rather to present a qualitative verification of the conclusion obtained in the preceding section. Thus, we consider the simplest “ohmic” model of the environment in the high-temperature approximation.<sup>5</sup> In this approximation the environment is described as an ensemble of harmonic oscillators.

The number of oscillators per unit frequency is proportional to the frequency in the region below the chosen “cutoff” frequency  $\Omega$  and  $k_B T \gg \hbar \Omega$ . The master equation for the density matrix  $\rho$  in the high-temperature approximation is

$$\begin{aligned} \frac{\partial \rho_{ss'}(z, z', \tau)}{\partial \tau} = & \left[ \frac{i}{2} \left( \frac{\partial^2}{\partial z^2} - \frac{\partial^2}{\partial z'^2} \right) - \frac{i}{2} (z^2 - z'^2) - \frac{\beta}{2} (z - z') \right. \\ & \times \left( \frac{\partial}{\partial z} - \frac{\partial}{\partial z'} \right) - D \beta (z - z')^2 - 2i\eta \\ & \left. \times (z' s' - z s) + i \dot{\varphi} (s' - s) \right] \rho_{ss'}(z, z', \tau) \\ & - i \frac{\epsilon}{2} [\rho_{s\bar{s}'}(z, z', \tau) - \rho_{\bar{s}s'}(z, z', \tau)]. \end{aligned} \quad (13)$$

Here,  $s, s' = \pm 1/2$ ,  $\bar{s} = -s$ ,  $\bar{s}' = -s'$ ,  $D = k_B T / \hbar \omega_c$ , and  $\beta = 1/Q$ , where  $Q$  is the quality factor of the cantilever. Again, we use the expansion over the eigenfunctions  $u_n$ ,

$$\rho_{s,s'}(z, z', \tau) = \sum_{n,m} A_{n,m}^{s,s'}(\tau) u_n(z) u_m^*(z'). \quad (14)$$

Next, we solve numerically the system of equations for the amplitudes  $A_{n,m}^{s,s'}(\tau)$ ,

$$\begin{aligned}
\dot{A}_{n,m}^{s,s'}(\tau) = & [i\dot{\varphi}(\tau)(s' - s) + \beta/2 - (n + m + 1)D\beta - i(n - m)] A_{n,m}^{s,s'}(\tau) - i\eta s' \sqrt{2m} A_{n,m-1}^{s,s'}(\tau) - i\eta s' \sqrt{2m+2} A_{n,m+1}^{s,s'}(\tau) \\
& + i\eta s \sqrt{2n} A_{n-1,m}^{s,s'}(\tau) + i\eta s \sqrt{2n+2} A_{n+1,m}^{s,s'}(\tau) + D\beta \sqrt{m(n+1)} A_{n+1,m-1}^{s,s'}(\tau) + D\beta \sqrt{n(m+1)} A_{n-1,m+1}^{s,s'}(\tau) \\
& + (D+1/2)\beta \sqrt{(n+1)(m+1)} A_{n+1,m+1}^{s,s'}(\tau) + (D-1/2)\beta \sqrt{nm} A_{n-1,m-1}^{s,s'}(\tau) - (D-1/2) \frac{\beta}{2} \sqrt{n(n-1)} A_{n-2,m}^{s,s'}(\tau) \\
& - (D+1/2) \frac{\beta}{2} \sqrt{(n+1)(n+2)} A_{n+2,m}^{s,s'}(\tau) - (D-1/2) \frac{\beta}{2} \sqrt{m(m-1)} A_{n,m-2}^{s,s'}(\tau) \\
& - (D+1/2) \frac{\beta}{2} \sqrt{(m+2)(m+1)} A_{n,m+2}^{s,s'}(\tau) - i \frac{\epsilon}{2} [A_{n,m}^{s,-s'}(\tau) - A_{n,m}^{-s,s'}(\tau)]. \tag{15}
\end{aligned}$$

Below we describe the results of our computer simulations for the values of parameters in Eq. (8). First, setting  $\beta = D = 0$  we obtain the density matrix  $\rho_{s,s'}(z, z', \tau)$  that exactly corresponds to the wave function  $\Psi(z, s, \tau)$  derived from the Schrödinger equation.

The initial density matrix is represented as a product of the cantilever and spin parts,

$$\rho_{s,s'}(z, z', 0) = \Psi(z, 1/2, 0) \Psi^*(z', 1/2, 0) \begin{pmatrix} 1 & 0 \\ 0 & 0 \end{pmatrix}. \tag{16}$$

The wave function  $\Psi(z, 1/2, 0)$  describes the quasiclassical state of the cantilever,

$$\Psi(z, 0) = \sum_{n=0}^{\infty} A_n(0) u_n(z). \tag{17}$$

The values  $A_n(0)$  are given in Eq. (7). The initial values  $A_{n,m}^{s,s'}(0)$  in Eq. (15) can be easily found from Eq. (16).

For  $\tau > 0$ , the density matrix describes the entangled state that cannot be represented as a product of the cantilever and spin parts. The initial peak of  $\rho_{s,s'}(z, z', \tau)$  splits into two peaks that are centered along the diagonal  $z = z'$ , and two peaks centered at  $z \neq z'$ , off the diagonal. The density matrix can be represented approximately as a sum of the four terms corresponding to the four peaks,

$$\rho_{s,s'}(z, z', \tau) = \rho_{s,s'}^{(1)} + \rho_{s,s'}^{(2)} + \rho_{s,s'}^{(3)} + \rho_{s,s'}^{(4)}, \tag{18}$$

where we omit variables,  $z, z', \tau$ . The matrices  $\rho^{(1)}$  and  $\rho^{(2)}$  describe the “big” and “small” diagonal peaks;  $\rho^{(3)}$  and  $\rho^{(4)}$  describe the peaks centered at  $z \neq z'$ .

As an illustration, we show in Fig. 3 the quantity,

$$|\rho_{1/2,1/2}(z, z', \tau) + \rho_{-1/2,-1/2}(z, z', \tau)|. \tag{19}$$

We have found that with accuracy to 1% the density matrix  $\rho_{s,s'}^{(1)}(z, z', \tau)$  can be represented as a product of the coordinate and spin parts,

$$\rho_{s,s'}^{(1)}(z, z', \tau) = \hat{R}^{(1)}(z, z', \tau) \hat{\chi}_{s,s'}^{(1)}(\tau), \tag{20}$$

where  $\hat{\chi}_{s,s'}^{(1)}(\tau)$  describes the spin that points in the direction of the external effective magnetic field  $[\epsilon, 0, -\dot{\varphi}(\tau)]$ . A simi-

lar expression is valid for  $\rho_{s,s'}^{(2)}(z, z', \tau)$ ; but in this case,  $\hat{\chi}_{s,s'}^{(2)}(\tau)$  describes a spin which points in the opposite direction.

First, we note that in order to describe the measurement process (the decoherence), we have to consider an ensemble

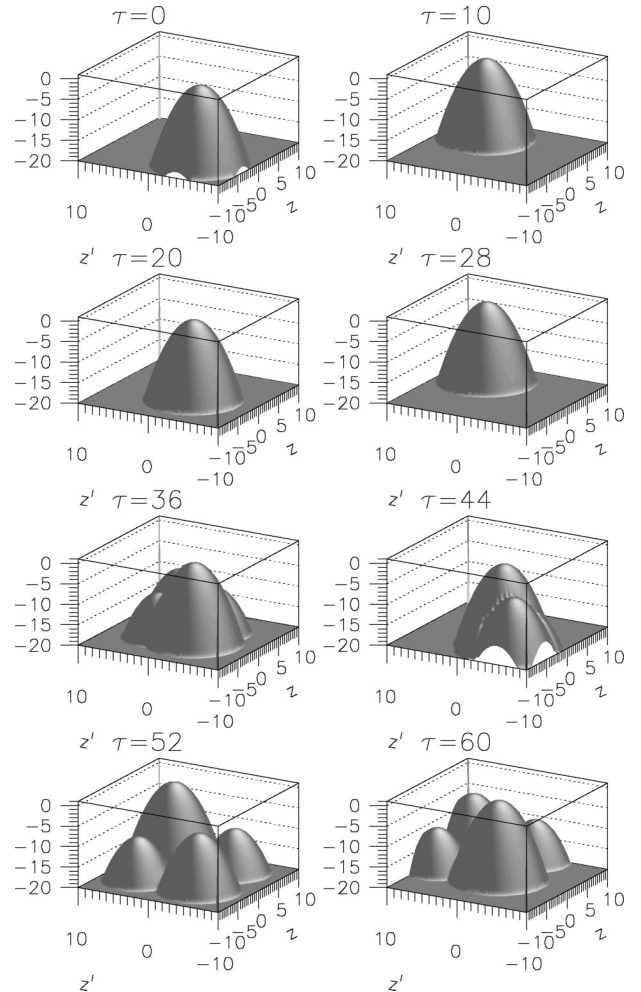


FIG. 3. Three-dimensional plot of  $\ln|\rho_{1/2,1/2}(z, z', \tau) + \rho_{-1/2,-1/2}(z, z', \tau)|$ , in the logarithmic scale. The values of parameters are  $\epsilon = 400$ ,  $\eta = 0.3$ ,  $\beta = D = 0$ . The initial conditions are  $\langle z(0) \rangle = -4$ ,  $\langle p_z(0) \rangle = 0$ .

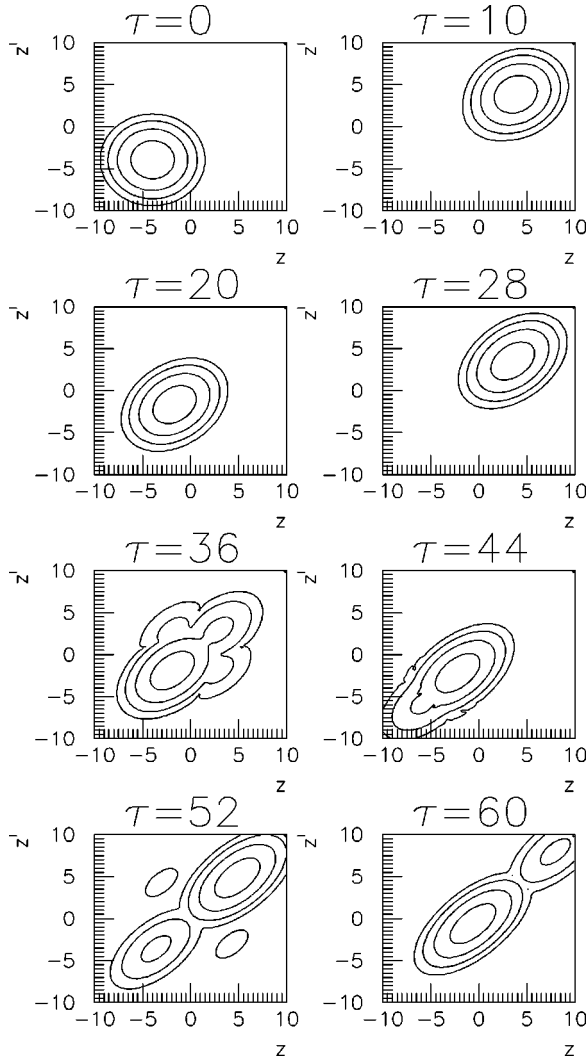


FIG. 4. The contours for  $\ln|\rho_{1/2,1/2}(z,z',\tau) + \rho_{-1/2,-1/2}(z,z',\tau)|$ . The values of parameters are  $\epsilon=400$ ,  $\beta=0.001$ , and  $D=10$ . The initial conditions are  $\langle z(0) \rangle = -4$ ,  $\langle p_z(0) \rangle = 0$ .

of quasiclassical cantilevers with the same initial conditions. At the same time, we are considering driven oscillations of the cantilever. So, the result of our simulations qualitatively does not depend on the initial conditions of the cantilever. Second, as we already mentioned, we are going to verify qualitatively the conclusion derived in the preceding section rather than simulate the expected experiment. Thus, we choose the values of parameters which help us to save a computational time. Namely, we choose a relatively small (but still quasiclassical) value for the initial energy of the cantilever, and a relatively small value for the thermal parameter  $D$  (without violating the high-temperature approximation which requires  $D \gg 1$ ). The small initial energy of the cantilever allows us to reduce the number of basis functions  $u_n(z)$ . A relatively small value of  $D$  allows us to observe four well-separated peaks at relatively small values of time,  $\tau$ .

The initial uncertainty of the cantilever position is  $\delta z = 1/\sqrt{2}$ . Due to thermal diffusion, the uncertainty of the can-

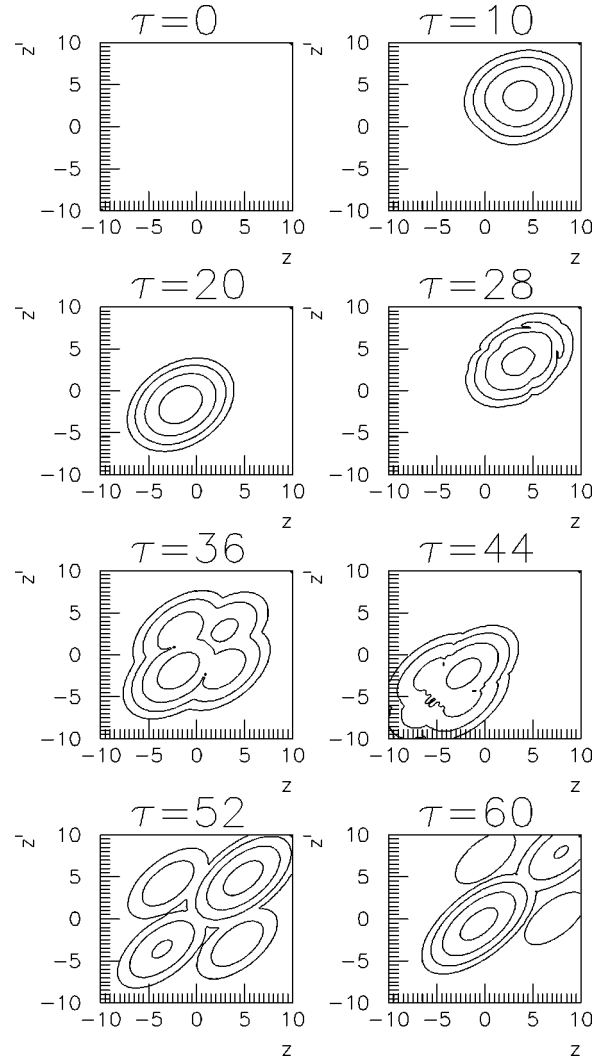


FIG. 5. The same as in Fig. 4, but for  $\ln|\rho_{1/2,1/2}(z,z',\tau) + \rho_{-1/2,-1/2}(z,z',\tau)|$ .

tiliver position increases with time. Thus, we have two effects: (i) the increase of the amplitude of the driven cantilever vibrations (similar to the Hamiltonian dynamics) and (ii) the increase of the uncertainty of the cantilever position due to thermal diffusion. If the second effect dominates, the two positions of the diagonal peaks (i.e., peaks centered on the line  $z=z'$ ) become indistinguishable. In this case, one cannot provide a spin measurement with two possible outcomes.

We have found that peaks centered on the diagonal retain the main properties described by the Hamiltonian dynamics. The density matrix  $\rho_{s,s'}^{(k)}(z,z',\tau)$  for  $k=1,2$  can be approximately represented as a product of the cantilever and spin parts. The spin part of the matrix describes the spin that points in the direction of the external effective magnetic field ( $k=1$ ) or in the opposite direction ( $k=2$ ).

Next, we discuss the two peaks centered at  $z \neq z'$ . As an illustration, Figs. 4 and 5 show the contours of the quantities

$$|\rho_{1/2,1/2}(z,z',\tau) + \rho_{-1/2,-1/2}(z,z',\tau)|$$

and

$$|\rho_{1/2,-1/2}(z,z',\tau) + \rho_{-1/2,1/2}(z,z',\tau)|$$

given in logarithmic scale. One can see the peaks centered at  $z \neq z'$  as well as at  $z = z'$ . The peaks centered at  $z \neq z'$  describe the coherence between the two cantilever positions. The amplitude of these peaks quickly decreases due to the decoherence. Thus, the master equation explicitly describes the process of measurement. The coherence between two cantilever trajectories (the macroscopic Schrödinger cat states) quickly disappears. As a result, the cantilever will “choose” one of two possible trajectories. Correspondingly (depending on the cantilever trajectory) the spin will point in the direction of the effective magnetic field or in the opposite direction.

#### IV. CONCLUSION

We have studied the quantum dynamics of the cantilever-spin system in a simple version of the CAI MRFM. In this version, the spin experiences a CAI under the action of the external phase-modulated rf magnetic field. If the frequency of CAI matches the cantilever frequency, the amplitude of the cantilever vibrations increases allowing single-spin detection. We have studied the problem: Which component of the spin is measured by the cantilever? We argue that one will measure the component of the spin along the direction of the effective magnetic field providing nondestructive de-

tection of the cantilever vibrations. This result was first derived using computer simulations of the Hamiltonian dynamics (the Schrödinger equation). Then, it was confirmed by the numerical solution of the master equation. We have considered the case when the amplitude of the driven cantilever vibrations was greater than the thermal noise. In this case, the phase of the driven vibrations depends on the spin component along the direction of the external effective magnetic field. Thus, detecting the phase of the cantilever vibrations, one can measure the spin component along the effective magnetic field.

We should mention that the direct relation between the cantilever trajectory and the direction of the spin has been verified for a transient process in the CAI MRFM. Our computer capabilities do not allow us to check this relation for the stationary cantilever vibrations at  $\tau \gg Q$ . Also, we completely ignored the direct interaction between the spin and the environment. We are now investigating this interaction.

#### ACKNOWLEDGMENTS

This work was supported by the U.S. Department of Energy (DOE) under the Contract No. W-7405-ENG-36. G.P.B. and VIT thank the National Security Agency (NSA), the Advanced Research and Development Activity (ARDA), and the Defense Advanced Research Projects Agency (DARPA) program MOSAIC for partial support.

<sup>1</sup>K. Wago, D. Botkin, C.S. Yannoni, and D. Rugar, Phys. Rev. B **57**, 1108 (1998).

<sup>2</sup>H.J. Mamin and D. Rugar, Appl. Phys. Lett. **79**, 3358 (2001).

<sup>3</sup>B.C. Stipe, H.J. Mamin, C.S. Yannoni, T.D. Stowe, T.W. Kenny, and D. Rugar, Phys. Rev. Lett. **87**, 277602 (2001).

<sup>4</sup>G.P. Berman, F. Borgonovi, G. Chapline, S.A. Gurvitz, P.C. Hammel, D.V. Pelekhov, A. Suter, and V.I. Tsifrinovich, quant-ph/0108025, J. Phys. A (to be published).

<sup>5</sup>A.O. Caldeira and A.J. Leggett, Physica A **121**, 587 (1983); Ann. Phys. (N.Y.) **149**, 374 (1983).